

Article

Parametric Investigation of Self-Centering Prestressed Concrete Frame Structures with Variable Friction Dampers

Linjie Huang , Zhendong Qian, Yuan Meng, Kaixi Jiang, Jingru Zhang and Chenxu Sang

College of Civil Engineering, Nanjing Forestry University, Nanjing 210037, China; zdong@njfu.edu.cn (Z.Q.); mengyuan@njfu.edu.cn (Y.M.); jiangkx@njfu.edu.cn (K.J.); 200650425@njfu.edu.cn (J.Z.); sangcx@njfu.edu.cn (C.S.)
* Correspondence: ljhuang@njfu.edu.cn

Abstract: To enhance the structural stiffness and energy-dissipating capacity after the decompression of beam-to-column connections for self-centering prestressed concrete (SCPC) frames, this study presents the seismic performance of a new type of SCPC frame with variable friction dampers (VFDs). The structure is characterized by a third stiffness and a variable energy-dissipating capacity. A 5-story and an 8-story VFD-SCPC frame were selected as the analytical cases, and their numerical models were built based on OpenSees 3.3.0 finite-element software. Sixteen ground-motion records were selected as excitations for the analyses, and the influence of the second stiffness and the third stiffness for the VFD-SCPC connections, as well as the second activation for VFD, on the seismic performance of the structures, was studied. The results showed that increasing the stiffness (number) of prestressed strands and their distance to the center of the beam section can obviously increase the second stiffness of the structures, thus decreasing their displacement, while the distribution mode of inter-story drift along the building's height cannot be changed. Increasing the third stiffness of the connections (the angle of slope sliding parts and the stiffness for the combination of disc springs) can effectively reduce the deformation of the structures under MCE (maximum-considered earthquakes) seismic levels and improve the energy-dissipation capacity of structures significantly. The premature secondary activation of VFD can enhance the loading capacity and energy-dissipation capacity of structures under both DBE (design-basis earthquakes) and MCE seismic levels, and reduce the inter-story drift of structures effectively.

Keywords: seismic performance; self-centering; variable friction dampers; nonlinear dynamic analysis; energy-dissipation capacity



Citation: Huang, L.; Qian, Z.; Meng, Y.; Jiang, K.; Zhang, J.; Sang, C. Parametric Investigation of Self-Centering Prestressed Concrete Frame Structures with Variable Friction Dampers. *Buildings* **2023**, *13*, 3029. <https://doi.org/10.3390/buildings13123029>

Academic Editors: Mizan Ahmed, Xiangyong Ni, Qin Zhang, Weiqing Zhu and Yantai Zhang

Received: 8 November 2023
Revised: 27 November 2023
Accepted: 4 December 2023
Published: 5 December 2023



Copyright: © 2023 by the authors. Licensee MDPI, Basel, Switzerland. This article is an open access article distributed under the terms and conditions of the Creative Commons Attribution (CC BY) license (<https://creativecommons.org/licenses/by/4.0/>).

1. Introduction

In recent decades, major earthquakes occurring around the world have caused severe damage and even collapse to structures [1–4]. Serious damage to the structural components and larger residual displacement of entire structures have caused huge economic losses [5–7]. Therefore, different types of structures have been developed to increase their seismic performance and decrease the economic losses caused by earthquakes [8–12]. Self-centering prestressed concrete (SCPC) frames, proposed by the PRESSS program, have been developed as a novel seismic-resistant system to enhance the resilience of structures due to minor residual drift under earthquakes [13]. Differing from traditional reinforced concrete frames, the beam and column of SCPC frames are assembled via prestressed strands and energy-dissipating devices. Under earthquakes, the energy-dissipating devices are activated by gap openings between the beams and columns to mitigate the damage to structural components. Recentring systems, such as prestressed strands [14], SMA [15], and fiber-reinforced polymers (FRP) [16–19], are used to mitigate the residual deformation of structures after earthquakes.

In terms of mitigating the damage to structural components, energy-dissipating technology has been improved. Priestly et al. [20] and Stone et al. [21] proposed early on

that connections be made by installing internal energy-dissipating properties. For the installation and disassembly, the energy-dissipating devices were installed into the external regions of the connections. For example, mild steel energy dissipators were anchored to connections and whole floors by Li et al. [22] and Pampanin et al. [23]. To achieve the expected energy-dissipation and self-centering capacity simultaneously, shape memory alloys (SMAs), characterized by hyperelasticity and high damping, have been used in the region of external connections by Youssef et al. [24] and Choi et al. [25].

To improve the efficiency of assembly and the shear resistance capacity of connections, angle steel was arranged at the top and bottom of the beam end by Lu et al. [26] and Sun et al. [27]. In addition, bolt-based friction dampers were gradually applied to the self-centering systems due to their simple construction and high recycling ratio. Veismoradi et al. [28] proposed the concept of installing self-centering rotational friction dampers on structures to adapt the rotational behavior of beam-to-column connections under earthquakes. Song et al. [29] proposed that an SCPC connection combined with friction dampers and steel jackets would effectively avoid compressive damage to local concrete during the gap-opening process of the connections.

With the continuous improvement of the aforementioned high-energy-consumption technology, the SCPC frame shows good performance under design-basis earthquakes (DBE). However, for these systems, as the beam-to-column connections decompress, the energy-dissipation systems are activated to dissipate energy; the stiffness of the connections is mainly controlled by the prestressed strands, and the stiffness of the structure is greatly weakened, resulting in the lateral displacement of the SCPC frame being significantly larger than that of cast-in-place concrete frames [30,31]. Furthermore, the energy-dissipating capacity is either constant or shows some degradation caused by the yield of energy-dissipating devices [32], which may not be sufficient for major earthquakes, thus resulting in structural damage. Rodgers et al. [33] and Kam and Pampanin [34] proposed that a reduction in stiffness and insufficient energy-dissipating capacity may stimulate the participation of higher modes, causing weak story damage and increasing the local displacement of structures. To enhance the structural stiffness after the decompression of beam-to-column connections, certain authors have proposed a variable friction-damped (VFD) SCPC connection [35] in which the slope friction configuration is used to provide greater stiffness and a higher energy-dissipating capacity when the structure experiences significant displacements. Differing from the hysteresis behavior of common SCPC frames, the VFD-SCPC connection presents three stages of stiffnesses and two instances of activation for dampers, as shown in Figure 1a. Although researchers have experimentally proven the good hysteresis behavior of VFD-SCPC connections, the influence of hysteresis parameters, such as third stiffness K_3 and second activation, on the seismic responses of structures has not yet been studied. The nonlinear dynamic analyses for a 5-story and 8-story building, using VFD-SCPC frames as lateral resistance systems, were carried out under design-basis earthquakes (DBE) and maximum-considered earthquakes (MCE) to study the hysteresis parameters of connections and their effects on the influence of seismic behavior for entire structures.

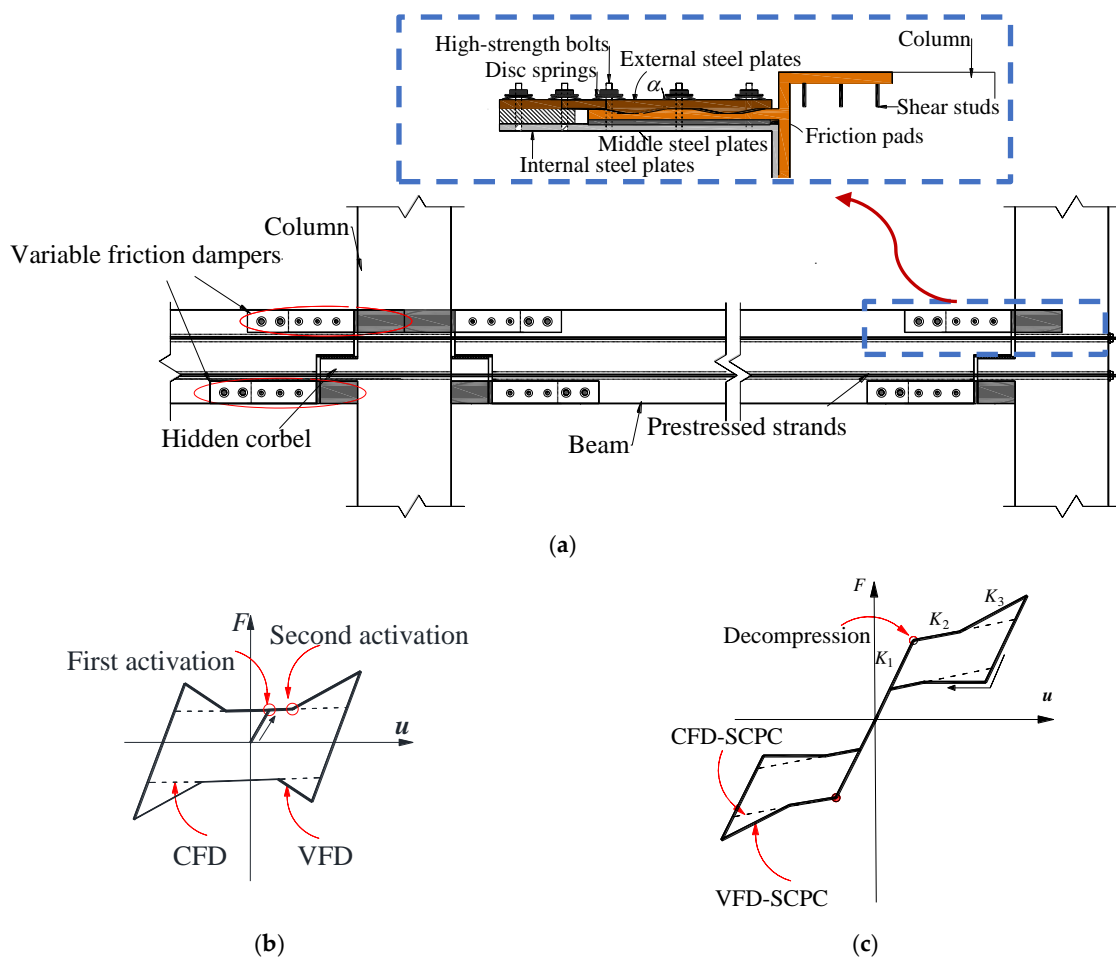


Figure 1. Configuration and mechanism of VFD-SCPC frames. (a) Configuration of VFD and VFD-SCPC frames. (b) Hysteretic curves of variable friction dampers. (c) Hysteretic curves of connections.

2. Configuration and Numerical Model of VFD-SCPC Connection

2.1. Connection Configuration of VFD-SCPC Connections

The configuration of VFD-SCPC frames is shown in Figure 1a. VFD consists of internal steel plates, middle steel plates, external steel plates, friction pads, high-strength bolts, and disc springs. Both the middle steel plates and external steel plates include flat and slope stages. When VFD is slid to the flat stage, the performance of VFD is the same as that of the constant friction dampers, whose friction force is theoretically constant. With the connection rocks open under lateral sway, a gap forms at the beam-to-column interface, thus causing the lateral stiffness of the system to decrease. When VFD is slid to the slope stage, corresponding to the second activation of VFD, the friction force is increased as the sliding distance increases, and a stiffness is formed, as shown in Figure 1b.

The friction pads are fixed to the internal friction steel plates. The key to achieving the expected seismic performance is a reliable design for VFD and its connection with beams and columns. The external and internal friction steel plates are connected to beams via high-strength bolts, while the middle friction steel plates are fixed to columns. The key to achieving variable friction behavior is that both the middle steel plates and external steel plates be comprised of a flat part and a slope part. Under earthquakes, relative deformation occurs between beams and columns, promoting relative sliding between the middle steel plate and the internal steel plate as well as the middle steel plate and the external steel plate. The hysteretic behavior of the VFD-SCPC connection is a combination of PT connections and VFD connections. Compared to common constant friction-damped (CFD) SCPC connections, a third stiffness is formed, as shown in Figure 1c. K_1 is the first stiffness of

connections, which is equal to the stiffness of the cast-in-situ beam-to-column connection theoretically. K_2 is the second stiffness of connections, which is mainly determined by the stiffness of prestressed strands. K_3 is the third stiffness of connections, which is determined by the angle for the slope stages of external steel plates and the stiffness of disc springs.

2.2. Finite-Element Model of Connection

Mechanism of the Interaction between Axial and Bending Deformations

The OpenSees (The Open System for Earthquake Engineering Simulation) [36] finite-element software was used to simulate the numerical model of VFD-SCPC connections, shown in Figure 2. All the beams and columns were simulated by the fiber-based nonlinear beam–column element to obtain the distributed plasticity characteristics. P-delta transformation was used to convert the geometrical coordinates of the columns to take into account the p-delta effect caused by the lateral displacement of the structure. The concrete for the beams and columns was simulated using the Uniaxial Material Concrete 02 constitutive model, which can consider the tension of concrete [36–40]; Longitudinal reinforced steel bars in beams and columns were modeled using a Steel 02 constitutive model, which was able to capture the hardening effect [41,42]. Prestressed strands were simulated by two Truss elements, which were parallel to the beam. The Steel 02 constitutive material assigned with an initial stress was attached to the Truss element to simulate the initial forces being applied to the prestressed strands. As shown in Figure 2, both the beam–column interfaces and the beam–corbel interfaces were simulated by a pair of rigid elements. A Zerolength contact element was assigned to the center of rotation to simulate the gap-opening and closing of the connection. Uniaxial Material ENT (elastic no-tension) material, which is characterized by compressive, but not tensile, behavior, was attached to the Zerolength contact element. The two points at the corbel–beam contact were coupled in the y-direction to simulate the transfer path of vertical shear force from beam to corbel.

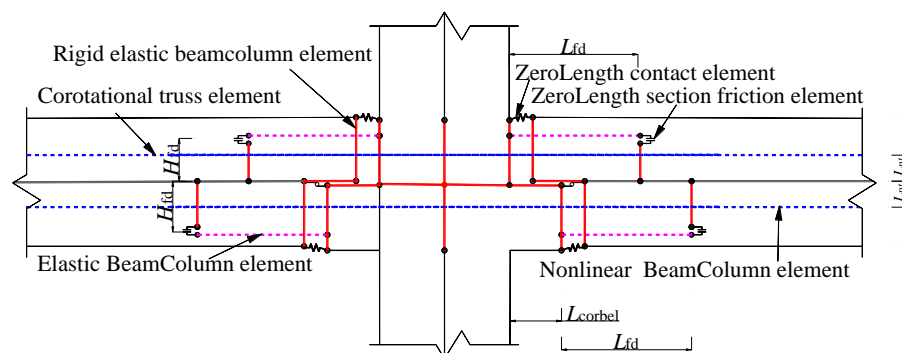


Figure 2. Numerical model based on OpenSees. Note: L_{fd} is the height and length for the external steel plates of friction dampers; H_{fd} is the distance between the center of friction dampers and the center of beams; L_{corbel} is the length of hidden corbels; L_{pt} is the distance between the prestressed strands and the center of beams.

The steel plate elements in VFD were modeled using a nonlinear beam–column element composed of Steel 02 material. One end of the steel plate element was connected to the column or corbel, and the other end was connected to the beam. Variable friction behavior was simulated using a Zerolength section element composed of the hysteretic material.

3. Prototype Buildings

To study the influence of the VFD-SCPC connection configuration on the seismic performance of self-centering frames, the prototype structure was selected as the study case, as shown in Figure 3a. The case study is referenced from a structure in which the SCPC frames are used as the lateral resistance systems, designed by Kam et al. [43]. Five-story and eight-story structures are commonly used in self-resetting concrete frame structures. A five-story floor and an eight-story VFD-SCPC frame designed according to the seismic

design method proposed by Huang [31] were utilized to study the controlling mechanism of variable friction behavior on higher mode effect structures after opening the gaps in the connections. The seismic intensity of the project site was VIII degree, with 0.2 g basic ground-motion acceleration for design-basis earthquakes (DBE) and a 10% probability of exceedance in 50 years [44]. Assuming the prototype structure is in the area of a stiff soil site, corresponding to a site class D according to GB50011-2010 [31]. This system is mainly composed of a moment-resisting frame and a gravity frame. During the design process, lateral load, such as lateral earthquake action, was mainly resisted by the moment-resisting frames. The floor-to-floor height of the first story and other stories were 4200 mm and 3600 mm, respectively. Six spans of beams of 6000 mm were arranged in each direction. The target seismic performance of the design structure was that under the DBE seismic level, the inter-story drift would not exceed 1.0%, and the main components, such as beams and columns, would all be kept elastic. Under the MCE seismic level, the inter-story drift did not exceed 2.0%, which is the limit of inter-story drift corresponding to serious damage stipulated by the Code for Seismic Design of Building (GB50011-2010) [44–46]. In addition, slight damage to the beams and columns is permitted from the perspective of economics, and the prestressed steel strands should be in the elastic range to ensure the reparability performance of structures under the MCE seismic level.

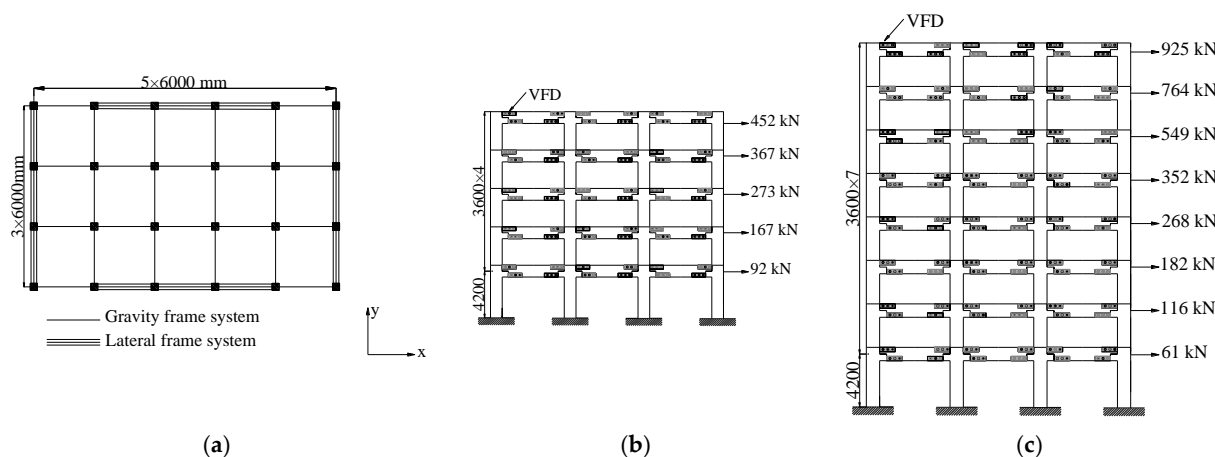


Figure 3. Prototype structures. (a) Plane layout. (b) Five-story structure. (c) Eight-story structure.

The concrete used in the beams and columns was C40 grade, with a compressive strength of 40 MPa; the longitudinal reinforcement was HRB335 grade, with a yield strength of 335 MPa and an ultimate strength of 540 MPa. The prestressed strands had a yield strength of 1675 MPa and an ultimate strength of 1860 MPa. The gravity loads for the five-story and eight-story structures were 45,360 kN and 72,500 kN, respectively. The gravity loads are applied to the beams in a distributed form. The story shear force for each VFD-SCPC frame is shown in Figure 3. Because the cost of connections using friction dampers is higher than that of reinforced concrete beam-to-column connection, using only the middle three bays or even fewer bays rather than all five bays of the outer side of the structure is an economical section. For a specific structure, the number of bays for the SCPC frame can be increased or decreased by controlling the total clamping force applied by all the friction bolts and designing prestressed strands.

The reinforcement and dimension of the beams and columns for the five-story and eight-story structures are shown in Tables 1 and 2, respectively, where B_b and H_b are the width and height of the beam section, respectively, B_c and H_c are the width and height of the column section, respectively, ρ_b and ρ_c are the reinforcement ratio of beam and column, respectively, and A_{ps} and $F_{ps,0}$ are the area and initial force of prestressed strands, respectively. F_C is the clamping force applied to high-strength bolts. K_{cds} is the stiffness for the combination of disc springs. The parametric analyses of the two structures were performed by changing the key design parameters to study the dynamic

response of VFD-SCPC frames. For convenience of comparison between structures with different parameters, the aforementioned five-story and eight-story structures, shown in Tables 1 and 2, are denoted as the benchmark frames, VFD-SCPC5-B and VFD-SCPC8-B, respectively. It should be noted that the arrangement of PT tendons in Figure 3 is the same as that in the configuration of connections shown in Figure 1.

Table 1. Design information of five-story VFD-SCPC frame.

Floor	Beam ($B_b \times H_b$) (mm)	Column ($B_c \times H_c$) (mm)	ρ_b (%)	ρ_c (%)	A_{ps} (mm ²)	$F_{ps,0}$ (kN)	F_C (kN)	$K_{c ds}$ (kN/mm)
1	400 × 650	600 × 600	0.66	1.86	1251	1202	205	18.3
2	400 × 600	600 × 600	0.71	2.18	1112	1209	206	19.8
3	400 × 600	550 × 550	0.71	1.91	1112	1131	192	18.6
4	400 × 550	550 × 550	0.76	2.27	973	980	167	17.4
5	400 × 550	550 × 550	0.76	1.94	834	718	122	12.8

Table 2. Design information of eight-story VFD-SCPC frame.

Floor	Beam ($B_b \times H_b$) (mm)	Column ($B_c \times H_c$) (mm)	ρ_b (%)	ρ_c (%)	A_{ps} (mm ²)	$F_{ps,0}$ (kN)	F_C (kN)	$K_{c ds}$ (kN/mm)
1	400 × 700	750 × 750	0.66	1.95	1793	1514	463	42.5
2	400 × 650	750 × 750	0.71	2.22	1673	1533	476	35.3
3	400 × 650	700 × 700	0.71	2.06	1679	1530	461	32.6
4	400 × 600	700 × 700	0.76	2.32	1455	1412	451	31.9
5	400 × 600	650 × 650	0.76	2.01	1324	1323	308	26.7
6	400 × 600	650 × 650	0.76	1.76	1120	1128	269	21.2
7	400 × 600	600 × 600	0.76	2.08	1003	943	229	18.3
8	400 × 600	600 × 600	0.76	2.06	918	635	135	13.4

4. Dynamic Time History Analyses

4.1. Selection of Ground-Motion Records

To evaluate the seismic performance of the VFD-SCPC frame and to study the influence of key parameters on the seismic performance of structures, combining the site features of the prototype structures and the principles relating to the selection method of ground-motion records stipulated by American ATC-63 (Applied Technology Council Project), 16 ground-motion records, which were selected from American PEER (The Pacific Earthquake Engineering Research Center) and the Wenchuan earthquake in China, were used as the excitations for the structure [36].

4.2. The Verification of Target Structural Seismic Performance

First, the aforementioned 16 ground-motion records were adjusted to DBE and MCE seismic levels as the excitations for our dynamic time history analyses. The adjustment approach consisted of scaling the spectral acceleration, $S_a(T_1, 5\%)$, of the average ground-motion spectrum to the spectral acceleration of the target seismic ground-motion level (DBE and MCE) at the point of the basic period (T_1). A comparison between the design spectrum and the target spectrum is shown in Figure 4a,b.

The maximum inter-story drift values of VFD-SCPC5-B and VFD-SCPC8-B under the DBE and MCE seismic levels are shown in Figures 5 and 6. The distribution of inter-story drift along the height of the building is also shown in Figures 5 and 6. It can be found that under the DBE and MCE seismic levels, only a few ground-motion records resulted in the maximum inter-story drift beyond the limit value. Under the DBE seismic level, the average inter-story drift of VFD-SCPC5-B was 0.78%, and this value was 0.75% for VFD-SCPC8-B. Under the MCE seismic level, the inter-story drift values for both the VFD-SCPC5-B and VFD-SCPC8-B were less than the limit value of 2.0%. The stress of the prestressed strands for VFD-SCPC5-B and VFD-SCPC8-B was less than the yield strength, indicating

that prestressed strands can always provide recentering forces to the system. It can be concluded that VFD-SCPC5-B and VFD-SCPC8-B met the target seismic performance under DBE and MCE seismic levels.

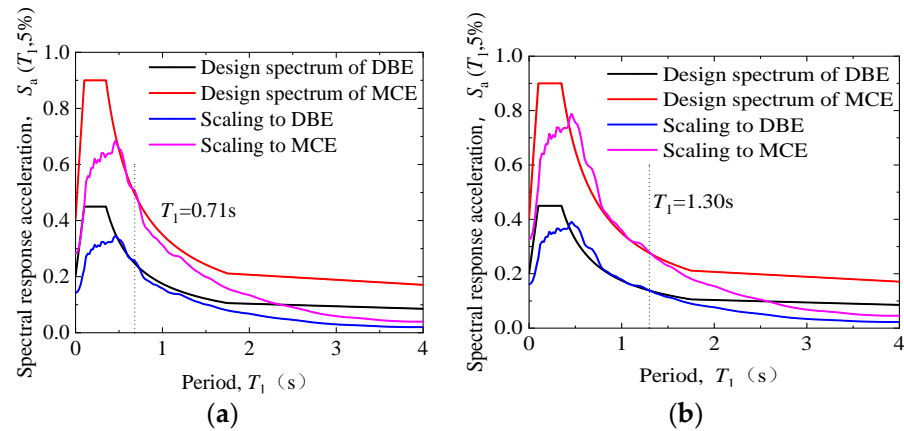


Figure 4. Ground-motion records scaled to design spectrum. (a) Five-story structure. (b) Eight-story structure.

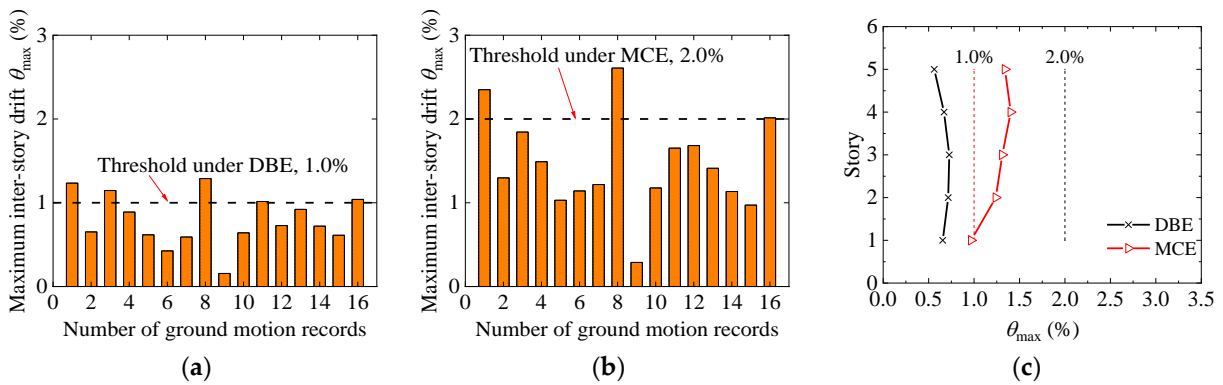


Figure 5. Dynamic response of VFD-SCPC5-B under ground-motion records. (a) DBE. (b) MCE. (c) Distribution of inter-story drift along building height.

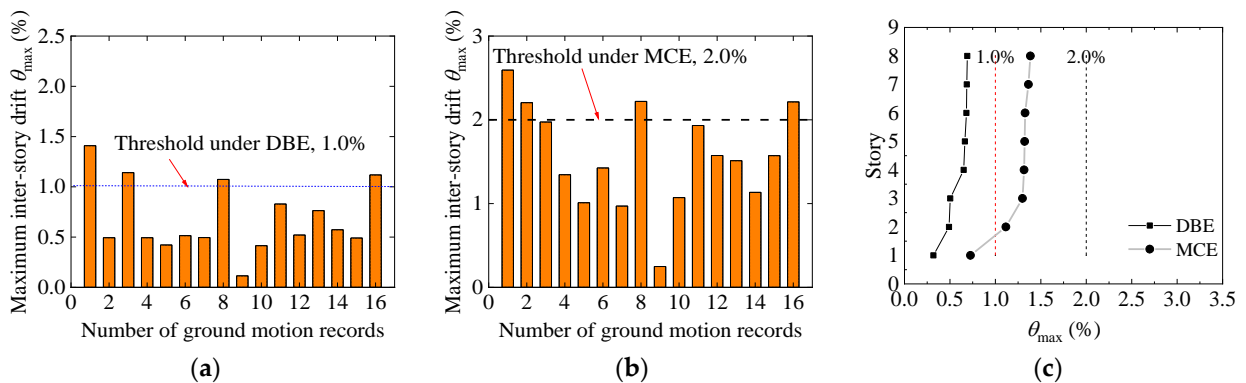


Figure 6. Dynamic response of VFD-SCPC8-B under ground-motion records. (a) DBE. (b) MCE. (c) Distribution of inter-story drift along building height.

Furthermore, it can be observed in Figures 5c and 6c that the distribution of inter-story drift along the height of the building varied with the increase in ground-motion intensity. For example, for VFD-SCPC5-B, the maximum inter-story drift was located on the third floor under the DBE seismic level but on the fourth floor under the MCE seismic level. With the increase in the number of structural floors, the distribution of inter-story drift along the

building's height presented different patterns. For VFD-SCPC8-B, under both the DBE and MCE seismic levels, the inter-story drift of the top floor was larger than that of other floors, which may have been caused by the contribution of a higher mode effect. It is indicated that the SCPC frames will present higher mode effects easily under major earthquakes, and the higher mode effect will be more obvious due to the increase in the number of structural floors and the increase in ground-motion intensity.

4.3. Analysis of the Impacts of Key Parameters on the Anti-Seismic Properties of Structures

The main difference between VFD-SCPC frames and common SCPC frames with constant friction forces is the multi-stage bearing capacity induced by VFD. When the VFD is at the flat slip stage, it is equivalent to a constant friction damper. The main influencing factor on friction force is the prestressed clamping force applied to the bolts because the influence of friction force on the seismic performance of SCPC frames has been verified by Song et al. [29]. Morgen and Kurama's [40] research emphasizes the influence of second stiffness, caused by the gap-opening of the beam-to-column connection, and third stiffness, caused by VFD, on the seismic performance of structures.

4.3.1. The Influence of Prestressed Strands on the Seismic Performance of VFD-SCPC Frames

The second stiffness of the SCPC frame is one of the most important factors that influence the seismic performance of structures after the gap-opening of the connections. According to Huang et al. [35], the second stiffness of connections can be changed through two methods: (1) changing the number (stiffness) of prestressed strands or (2) changing the distance of the prestressed strands to the center of the beam section. Therefore, the number of prestressed strands and the distance of the prestressed strands to the center of the beam section were changed to analyze the seismic responses of the structures. The stiffness of the prestressed strands was scaled by two times compared to the benchmark structures (VFD-SCPC5-B and VFD-SCPC8-B), and the contrast models corresponding to the five-story and eight-story buildings were recorded as VFD-SCPC5-PT2 and VFD-SCPC8-PT2, respectively. The prestressed strands were arranged on the upper and lower sides of the beam ($\pm 1/4$ times the beam section height), while their total area remained unchanged. The contrast models corresponding to five-story and eight-story buildings were recorded as VFD-SCPC5-PH1/4 and VFD-SCPC8-PH1/4, respectively.

Figure 7 presents the maximum inter-story drift of the structures under DBE and MCE seismic levels. Moreover, the average values of the inter-story drift for each model under the 16 ground-motion records are shown in Table 3. It can be found that the inter-story drift of these contrast models (VFD-SCPC5-PT2, VFD-SCPC5-PH1/4, VFD-SCPC8-PT2, and VFD-SCPC8-PH1/4) decreased to different degrees in comparison to VFD-SCPC5-B and VFD-SCPC8-B. It is believed that the stiffness contribution of prestressed strands for these contrast models is greater than that for the benchmark models (VFD-SCPC5-B and VFD-SCPC8-B), meaning that the stiffness of the contrast models after the opening of the gaps is greater than that of the benchmark models. Moreover, to analyze the reducing effect of the two methods involving changing the second stiffness of the inter-story drift of the structures, the variation rate of the inter-story drift of the contrast model compared to the benchmark models (VFD-SCPC5-B and VFD-SCPC8-B) was calculated. We found that under the DBE seismic level, the variation in the stiffness of the prestressed strands does not cause an obvious change in the dynamic responses of structures. For example, the inter-story drift of the contrast model decreased by less than 10% compared to benchmark models.

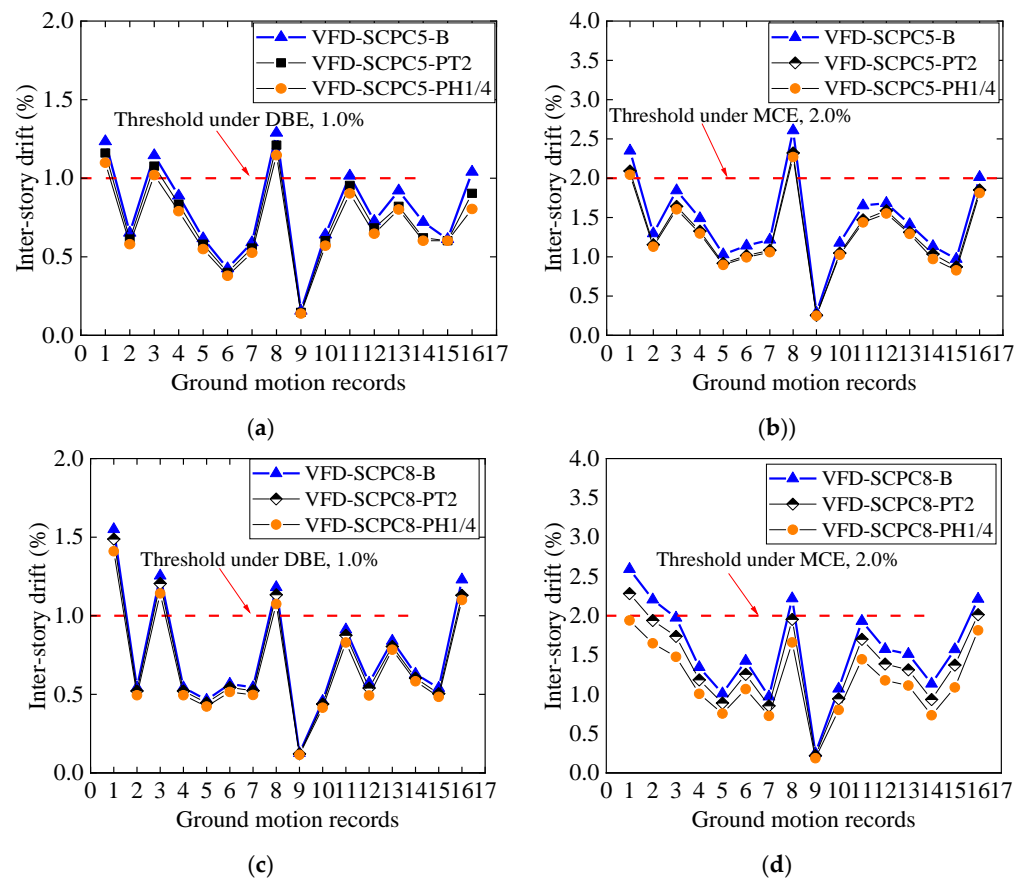


Figure 7. Inter-story drift of structures with different second stiffness under 16 ground-motion records. (a) DBE (Five-story buildings). (b) MCE (Five-story buildings). (c) DBE (Eight-story buildings). (d) MCE (Eight-story buildings).

Table 3. Average inter-story drift of structures with different second stiffness.

Structure	Model	DBE		MCE	
		Average	Variation Rate	Average	Variation Rate
Five-story building	VFD-SCPC5-B	0.78%	-	1.46%	-
	VFD-SCPC5-PT2	0.74%	-5.13%	1.31%	-10.27%
	VFD-SCPC5-PH1/4	0.71%	-8.97%	1.28%	-12.33%
Eight-story building	VFD-SCPC 8-B	0.75%	-	1.56%	-
	VFD-SCPC 8--PT2	0.71%	-5.33%	1.40%	-10.26%
	VFD-SCPC8-PH1/4	0.68%	-9.33%	1.20%	-23.08%

Figure 8 presents the distribution of inter-story drift along the building's height. It can be observed that the distribution of inter-story drift along the building's height was unchanged as the stiffness of the prestressed strands varied. For each story, the change in inter-story drift of the contrast models decreased proportionally compared to the benchmark models.

However, under the MCE seismic level, both methods of increasing the second stiffness of the structure caused apparent decreases in the inter-story drift. Compared to the benchmark modes (VFD-SCPC5-B and VFD-SCPC8-B), the inter-story drift of the contrast model decreased by more than 10%, and the distribution of inter-story drift along the building's height showed an obvious difference. Moreover, for the contrast model, the reduction in inter-story drift for the higher floor was obviously larger than that for the lower floor. The inter-story drift of the lower floors showed a slight increase; thus, the distribution of inter-story drift along the building's height showed a more uniform trend.

It is indicated that increasing the second stiffness of structures can reduce higher modal effects under the MCE seismic level.

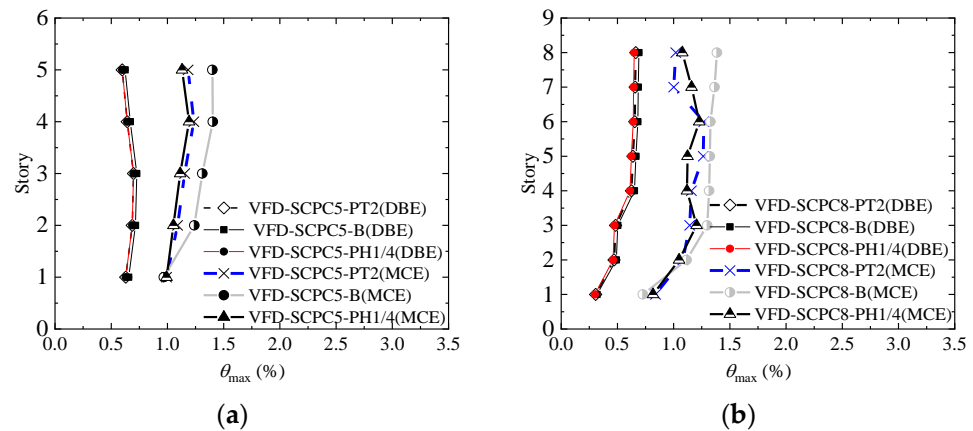


Figure 8. Inter-story drift of structures with different second stiffness along building height. (a) Five-story structures. (b) Eight-story structures.

Based on consideration of construction and cost, increasing the number of prestressed strands may raise the economic cost. However, the method of enlarging the arm of force for prestressed strands only requires adding one or more holes to be used to cross the prestressed strands during construction, which is an easy operation. We concluded that if the method of increasing the second stiffness of the connection were adopted to reduce the inter-story drift of structures, enlarging the location of the prestressed strands (arranged in the upper and lower parts of the beam) would be more economical.

4.3.2. The Influence of Slope Sliding Friction Parts on the Seismic Performance of VFD-SCPC Frames

The difference between the VFD-SCPC connection and the common CFD-SCPC connection is the third stiffness, which is mainly determined by the slope angle of the VFD and the stiffness of the disc springs. Therefore, compared to VFD-SCPC5-B and VFD-SCPC8-B, adjusting the slope angle of the VFD and the number of disc springs to reduce the third stiffness of VFD by 30% and increase it by 30% would correspond to 0.7 times and 1.3 times the third stiffness of the contrast models (VFD-SCPC5-B and VFD-SCPC8-B). These can be recorded as VFD-SCPC5-0.7K3, VFD-SCPC5-1.3K3, VFD-SCPC8-0.7K3, and VFD-SCPC8-1.3K3 to analyze the influence of the third stiffness on the seismic performance of structures. Figure 9 presents the maximum and average inter-story drift of contrast models and benchmark models under DBE and MCE seismic levels. The distribution of inter-story drift along the building's height is shown in Figure 10.

According to Figure 9, under the DBE seismic level, the inter-story drift of the benchmark models (VFD-SCPC5-B and VFD-SCPC 8-B) under a few ground-motion records exceeded 1.0%. The VFD entered the slope slide area, and the dynamic response of the structures was mainly affected by the third stiffness of the connections. Therefore, with the increase in the third stiffness, the inter-story drift of the structures was significantly reduced under the excitation of these ground-motion records. Conversely, the inter-story drift of the structure significantly increased as the third stiffness decreased. However, when the inter-story drift of the structure exceeded 1.0%, the target limit under DBE, the seismic performance of the structures was mainly controlled by the flat part of VFD. In this case, the dynamic response of the contrast models was almost equal to that of the benchmark models. Under the MCE seismic level, most of the ground-motion records resulted in the VFD on the floor with the largest displacement response entering the slope slide areas. The dynamic responses of the structures were mainly influenced by the third stiffness, so the dynamic response of the contrast models and benchmark models showed obvious

differences under most of the ground-motion records. The inter-story drift decreased with the increase in the third stiffness.

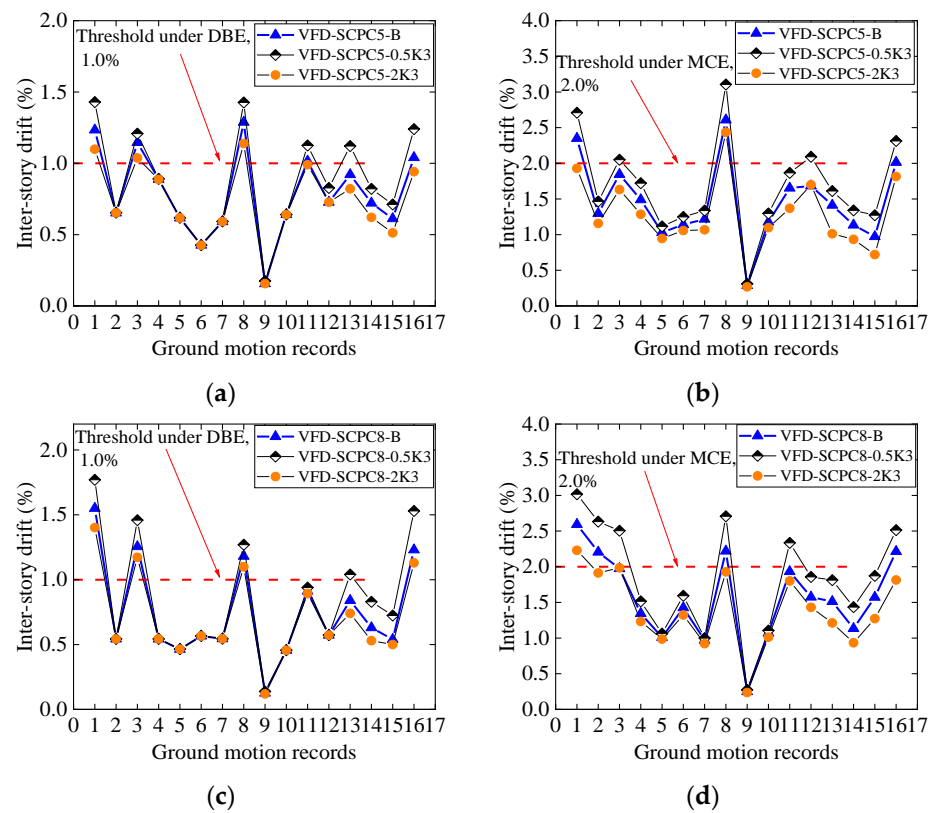


Figure 9. Inter-story drift of structures with different third stiffness under 16 ground-motion records. (a) DBE (Five-story buildings). (b) MCE (Five-story buildings). (c) DBE (Eight-story buildings). (d) MCE (Eight-story buildings).

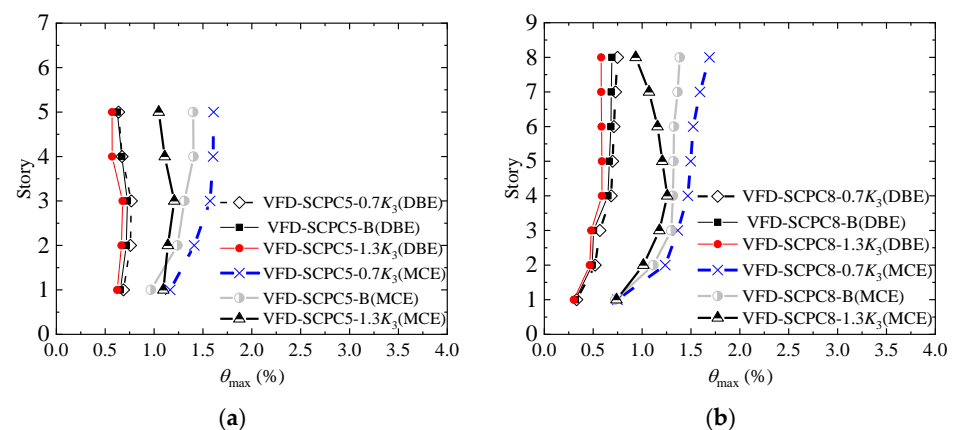


Figure 10. Inter-story drift of structures with different third stiffness along building height. (a) Five-story buildings. (b) Eight-story buildings.

It can be seen from Table 4 that under the DBE seismic level, compared to VFD-SCPC5-B, the inter-story drift for VFD-SCPC5-0.7K3 and VFD-SCPC5-1.3K3 was increased by 5.13% and reduced by 6.76%, respectively. Compared to VFD-SCPC 8-B, inter-story drift for VFD-SCPC 8-0.7K3 and VFD-SCPC 8-1.3K3 increased by 9.67% and reduced by 8.67%, respectively. Under the MCE seismic level, compared to the benchmark models, the variation in inter-story drift was obviously increased. The inter-story drift of VFD-SCPC5-0.7K3 and VFD-SCPC5-1.3K3 increased by 15.07% and reduced by 12.33%, respectively

and compared to VFD-SCPC8-B, VFD-SCPC8-0.7K3, and VFD-SCPC8-1.3K3 increased by 19.23% and reduced by 17.91%, respectively. Under both the DBE and MCE seismic levels, the variation rate of inter-story drift caused by the third stiffness in the eight-story buildings is higher than that in the five-floor buildings. It is indicated that the controlling effect of the third stiffness on the displacement of the structure under the DBE seismic level was less than that under the MCE seismic level. The control effect of the third stiffness on the displacement of the structure became better as the total number of floors increased.

Table 4. Average inter-story drift of structures with different third stiffness.

Structure	Model	DBE		MCE	
		Average	Variation Rate	Average	Variation Rate
Five-story building	VFD-SCPC5-B	0.78%	-	1.46%	
	VFD-SCPC5-0.7K ₃	0.82%	5.13%	1.68%	15.07%
	VFD-SCPC5-1.3K ₃	0.73%	-6.76%	1.28%	-12.33%
Eight-story building	VFD-SCPC 8-B	0.75%	-	1.56%	
	VFD-SCPC 8-0.7K ₃	0.83%	9.67%	1.86%	19.23%
	VFD-SCPC 8-1.3K ₃	0.69%	-8.67%	1.28%	-17.91%

It can be seen from Figure 10 that, under the DBE and MCE seismic levels, the distribution of inter-story drift along the building height for the contrast models and the benchmark models did not show obvious differences. Only as the third stiffness increased did the inter-story drift of each floor show a slight decrease. Under MCE seismic levels, the distribution of inter-story drift along the building's height showed an obvious difference between the contrast models and benchmark models. With the increase in the third stiffness, the inter-story drift of the upper floors was obviously reduced. For example, compared to VFD-SCPC8-B, the higher modal effect of VFD-SCPC8-1.3K3 was obviously reduced, while it increased for VFD-SCPC8-0.7K3, indicating that utilization of the greater third stiffness provided by slope section of VFD can effectively reduce the higher modal effects of structures. On the other hand, under the DBE seismic level, a higher modal effect did not show an obvious reduction, meaning that the second stiffness is not sensitive to the higher modal effects of structures. Therefore, it can be concluded from the above analysis that the third stiffness is sensitive to the responses of structures under the MCE seismic level, while it is not sensitive to the seismic responses of structures under the DBE seismic level.

4.3.3. The Influence of Secondary Activation of VFD on the Seismic Performance of Structures

Considering that oversized flat sliding parts of VFD may cause the slope sliding areas not to be activated, its effect is the same as that of the constant friction dampers. If the slope sliding area is activated prematurely, the seismic requirements of different seismic levels may be satisfied, although the design may be conservative, and the cost may be enhanced. Therefore, the key to achieving multi-stage seismic resistance of VFD-SCPC frames is designing the activation of slope parts for VFD. We took the secondary activation of VFD to be variable to study the seismic performances of structures. Defining the ratio between the length of the flat sliding area and the slope sliding area, α , we quantified the design needed to activate the slope sliding area. For benchmark models, α was equal to 0.55. In comparing the benchmark models, the inter-story drift corresponding to the activation of the slope sliding part varied between 0.7% and 1.3%, with α values of 0.31 and 0.94, respectively. Corresponding structures were recorded as VFD-SCPC5- α 0.31 (and VFD-SCPC8- α 0.31) and VFD-SCPC5- α 0.94 (and VFD-SCPC8- α 0.94), respectively. Figure 11 presents the maximum inter-story drift of the structures under the DBE and MCE seismic levels. Table 5 shows the average inter-story drift under 16 ground-motion records.

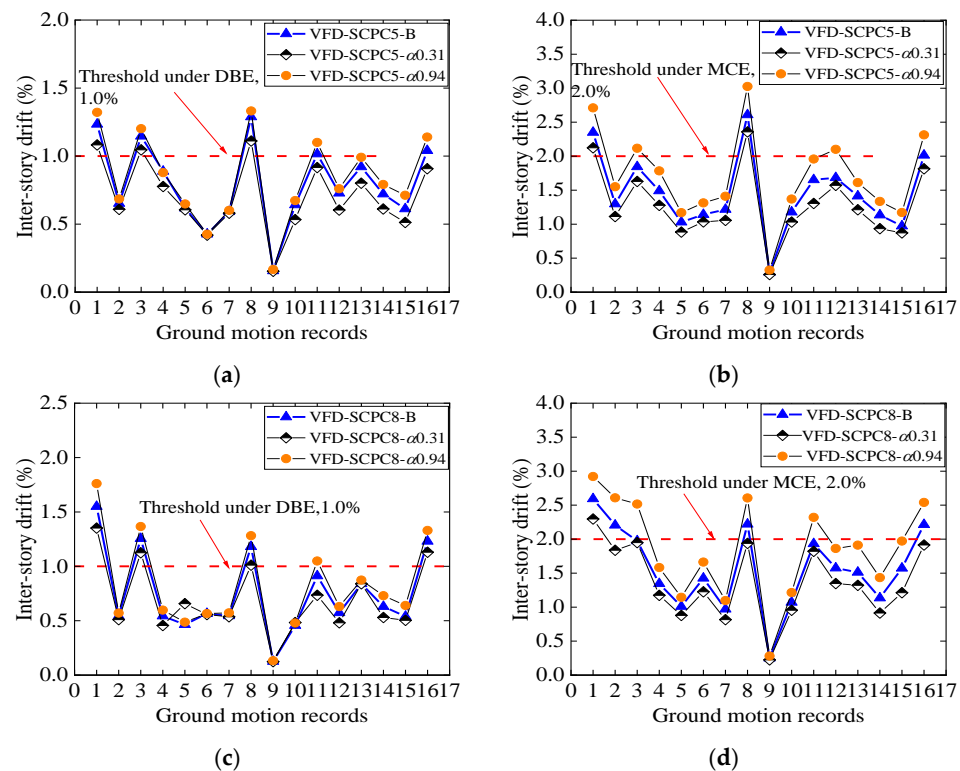


Figure 11. Inter-story drift of structures under 16 ground-motion records. (a) DBE (five-story structures). (b) MCE (five-story structures). (c) DBE (eight-story structures). (d) MCE (eight-story structures).

Table 5. Average inter-story drift.

Structure	Model	DBE		MCE	
		Average	Variation Rate	Average	Variation Rate
Five-story building	VFD-SCPC5-B	0.78%	-	1.46%	-
	VFD-SCPC5- α 0.31	0.71%	-8.97%	1.28%	-12.33%
	VFD-SCPC5- α 0.94	0.84%	7.69%	1.70%	16.44%
Eight-story building	VFD-SCPC 8-B	0.75%	-	1.56%	-
	VFD-SCPC 8- α 0.31	0.69%	-8.00%	1.36%	-12.82%
	VFD-SCPC 8- α 0.94	0.82%	9.33%	1.85%	18.59%

It can be observed that the inter-story drift for VFD-SCPC5- α 0.31 and VFD-SCPC8- α 0.31 was obviously smaller than that for the benchmark models, VFD-SCPC5-B and VFD-SCPC8-B ($\alpha = 0.55$), under both the DBE and MCE seismic levels. However, the inter-story drift values of VFD-SCPC5- α 0.94 and VFD-SCPC8- α 0.94 were the same as those of the benchmark models. This is because, under the DBE seismic level, the VFD for VFD-SCPC5- α 0.94 and VFD-SCPC8- α 0.94 slipped at the flat sliding areas under most of the ground-motion records. Under the MCE seismic level, for VFD-SCPC5- α 0.94 and VFD-SCPC8- α 0.94, VFD still slipped at the flat sliding areas under most of the ground-motion records, although the inter-story drift did not show obvious differences to the benchmark models. But for VFD-SCPC5- α 0.31 and VFD-SCPC8- α 0.31, the second activation of VFD occurred earlier than that of the benchmark models. The key influencing factors were the slope sliding areas, so the inter-story drift of VFD-SCPC5- α 0.31 was less than that of VFD-SCPC5-B, and the inter-story drift of VFD-SCPC8- α 0.31 was less than that of VFD-SCPC8-B.

According to Figure 12, with the change in the secondary activation of VFD, the distribution of inter-story drift along the building's height showed an obvious change, especially for higher floors in the structures. For the five-story structures, under both DBE

and MCE seismic levels, the inter-story drift of VFD-SCPC5- α 0.31 obviously decreased from the fourth to the fifth stories. For the eight-story structures, compared to VFD-SCPC8-B, the inter-story drift of VFD-SCPC8- α 0.31 for higher floors was lower than that for other stories under both the DBE and MCE seismic levels. This indicates that the premature activation of slope slipping areas of VFD can explain the higher modal effects of SCPC frames under both DBE and MCE seismic levels. On the other hand, compared to VFD-SCPC8-B, VFD-SCPC8- α 0.94 showed a more obviously higher modal effect under both DBE and MCE seismic levels. Therefore, the appropriate design of the second activation of VFD is useful for controlling the higher-order modal effects of SCPC frames under both DBE and MCE seismic levels.

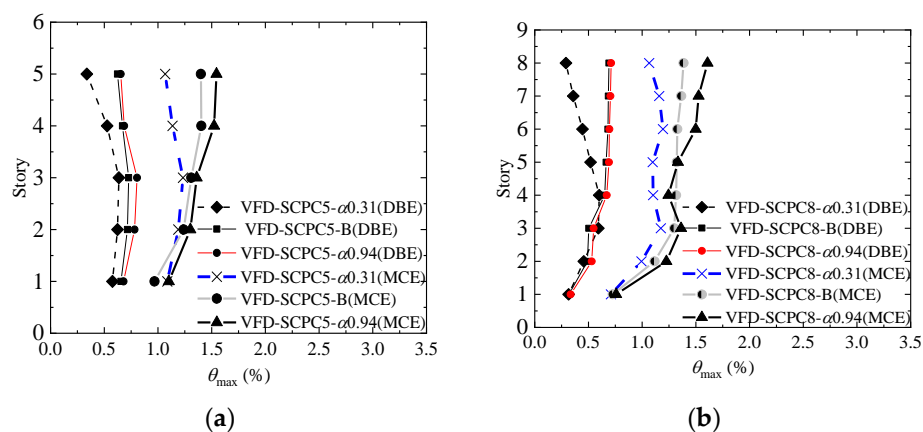


Figure 12. Inter-story drift of structures along building height. (a) Five-story buildings. (b) Eight-story buildings.

5. Conclusions

To study the influence of the hysteresis parameters of variable friction-damped SCPC connections on the seismic behavior of entire structures, nonlinear dynamic analyses for 5-story and 8-story buildings were carried out under design-basis (DBE) and maximum-considered earthquakes (MCE). The effects of the second stiffness, the third stiffness, and the secondary activation of variable friction dampers on the dynamic responses of structures, such as the inter-story drift, the floor deformation mode, and the higher modal effect, were studied. The following conclusions can be drawn:

- (1) Two methods can be used to improve the second stiffness of SCPC connections, which are increasing the stiffness (number) of the prestressed strands and increasing the force arm of the prestressed strands. Under the DBE seismic level, increasing the second stiffness had little effectiveness in terms of reducing the deformation of structures, while it had a significant effect under the MCE seismic level. The method of increasing the number of prestressed strands may increase the economic cost, while the method of increasing the force arm of prestressed strands is easy to implement and has a lower economic cost.
- (2) Increasing the third stiffness of the connections (the angle of slope sliding areas and the stiffness of the combination of disc springs) can effectively reduce the deformation of structures under MCE seismic levels. The energy-dissipation capacity of structures can also be significantly improved, and the higher mode effect of the structures can also be reduced. However, under DBE seismic levels, the loading capacity of the structures was mainly controlled by the flat sliding areas of VFD. The improvement of the third stiffness had almost no effect on the floor deformation or energy-dissipation capacity, and the higher modal effect could not be controlled effectively.
- (3) Reducing the length ratio of the flat sliding areas to the slope sliding areas ($\alpha = \Delta f / \Delta s$) can result in the secondary activation of VFD being performed prematurely. The loading capacity and energy-dissipation capacity of structures can be effectively im-

proved under both DBE and MCE seismic levels, the inter-story drift can be effectively reduced, and the higher modal effects can be significantly controlled. Therefore, in practical engineering, the secondary activation of VFD and the design of the third stiffness can be combined to control the higher modal effects of SCPC frames under both DBE and MCE seismic levels.

It should be noted that the derived conclusion is only accurate to the assumed case study of the 5- and 8-story frame in this study. For another structure with different dimensions and configurations, the conclusion should be modified based on more analyses, which will be carried out in the next steps of this ongoing research.

Author Contributions: Conceptualization, L.H. and Z.Q.; Software, L.H. and Y.M.; Validation, K.J.; Formal analysis, J.Z.; Investigation, K.J.; Resources, Y.M.; Data curation, C.S. All authors have read and agreed to the published version of the manuscript.

Funding: The research described in this paper was sponsored by the National Natural Science Foundation of China (52208480), the China Postdoctoral Science Foundation(2023M731712), Natural Science Foundation of the Jiangsu Higher Education Institutions of China (22KJB560007), Doctor of Entrepreneurship and Innovation in Jiangsu Province (JSSCBS20210553), Nanjing Forestry University Undergraduate Innovation Training Program (202210298100Y). These supports are gratefully acknowledged.

Data Availability Statement: The data are not publicly available due to privacy. The data presented in this study are available on request from the corresponding author.

Conflicts of Interest: The authors declare no conflict of interest.

References

1. Wen, J.; Li, X.; Xie, Q. Seismic disadvantages and formation mechanism of weak coupling effects in interconnected power infrastructures. *Soil Dyn. Earthq. Eng.* **2023**, *173*, 108082. [[CrossRef](#)]
2. Ouyang, X.; Zhang, Y.; Ou, X.; Shi, Y.; Liu, S.; Fan, J. Seismic fragility analysis of buckling-restrained brace-strengthened reinforced concrete frames using a performance-based plastic design method. *Structures* **2022**, *43*, 338–350. [[CrossRef](#)]
3. Zhang, Y.; Ouyang, X.; Sun, B.; Shi, Y.; Wang, Z. A comparative study on seismic fragility analysis of RC frame structures with consideration of modeling uncertainty under far-field near-field ground motion excitation. *Bull. Earthq. Eng.* **2022**, *20*, 1455–1487. [[CrossRef](#)]
4. Zhang, Y.; Sun, B.; Shi, Y.; Wang, Z. Estimation of Aleatory Randomness by Sa(T1)-Based Intensity Measures in Fragility Analysis of Reinforced Concrete Frame Structures. *CMES-Comput. Model. Eng. Sci.* **2022**, *130*, 73–96. [[CrossRef](#)]
5. Sun, B.; Zeng, Z.; Zhang, Y.; Shen, W.; Ou, J. An effective geometric nonlinear analysis approach of framed structures with local material nonlinearities based on the reduced-order Newton-Raphson method. *Soil Dyn. Earthq. Eng.* **2023**, *172*, 107991. [[CrossRef](#)]
6. Lin, Y.; Wang, Y.; Wu, W. Experimental study on PSPC beam–Concrete encased CFST column frame installed with novel steel panel dampers. *Eng. Struct.* **2023**, *288*, 116211. [[CrossRef](#)]
7. Lin, Y.; He, X.; Igarashi, A. Influence of directionality of spectral-compatible Bi-directional ground motions on critical seismic performance assessment of base-isolation structures. *Earthq. Eng. Struct. Dyn.* **2022**, *51*, 1477–1500. [[CrossRef](#)]
8. Wei, Y.; Nie, Y.; Lin, Y. Axial stress–strain behaviour of bamboo composite tube-confined recycled aggregate concrete with different aggregate replacement ratios. *Wood Mater. Sci. Eng.* **2023**, 1–17. [[CrossRef](#)]
9. Wu, F.; Wei, Y.; Lin, Y. Experimental study of bamboo scrimber-filled steel tube columns under axial compression. *Eng. Struct.* **2023**, *280*, 115669. [[CrossRef](#)]
10. Wu, F.; Wei, Y.; Lin, Y. Confinement effectiveness of bamboo scrimber-filled steel tube columns under axial compression. *J. Build. Eng.* **2023**, *68*, 106157. [[CrossRef](#)]
11. Guan, D.; Peng, Z.; Lin, Y. Development and seismic performance of precast rocking walls with multiple steel energy dissipaters. *Case Stud. Constr. Mater.* **2023**, *19*, e02304. [[CrossRef](#)]
12. Cao, Q.; Wei, Y.; Chen, S. Experimental investigations on the load-bearing properties of dowel connection joints of bamboo scrimber. *Structures* **2023**, *50*, 1868–1878. [[CrossRef](#)]
13. Priestley, M.J.N. Overview of press research program. *PCI J.* **1991**, *36*, 50–57. [[CrossRef](#)]
14. Song, G.; Yang, T.; Zhou, Y. Distribution of hysteretic energy demands in self-centering concrete frames with hybrid joints. *Soil Dyn. Earth. Eng.* **2021**, *148*, 106828. [[CrossRef](#)]
15. Qiu, C.; Liu, J.; Jiang, T.; Du, X. Experimental study on a steel self-centering rocking column with SMA slip friction dampers. *Eng. Struct.* **2022**, *274*, 115126. [[CrossRef](#)]
16. Wang, Y.; Zhou, Z.; Xie, Y.; Huang, L.; Zheng, J. Shake Table Tests of Self-Centering Steel Braced Frame with Pretensioned Basalt Fiber Reinforced Polymers. *J. Earthq. Eng.* **2022**, *27*, 3251–3268. [[CrossRef](#)]

17. Liu, J.; Yuan, Y.; Wang, L.; Liu, Z.; Yang, J. Parameter Study of Interfacial Capacities for FRP–Steel Bonded Joints Based on 3D FE Modeling. *Materials* **2022**, *15*, 7787. [[CrossRef](#)]
18. Liu, J.; Guo, T.; Wei, Y.; Wang, L.; Zou, X. Investigation of the Effect of Pre-Tightening Forces on Bolted Connection for FRP–Steel Joints. *Case Stud. Constr. Mater.* **2023**, *19*, e02348. [[CrossRef](#)]
19. Wang, G.; Wei, Y.; Shen, C.; Huang, Z.; Zheng, K. Compression performance of FRP–steel composite tube-confined ultrahigh-performance concrete (UHPC) columns. *Thin-Walled Struct.* **2023**, *192*, 111152. [[CrossRef](#)]
20. Priestley, M.J.N.; Tao, J.R. Seismic response of precast prestressed concrete frames with partially debonded tendons. *PCI J.* **1993**, *38*, 58–69. [[CrossRef](#)]
21. Stone, W.C.; Cheok, G.S.; Stanton, J.F. Performance of hybrid moment-resisting precast beam–column concrete connection subjected to cyclic loading. *ACI Struct. J.* **1995**, *92*, 229–249.
22. Li, L.; Mander, J.B.; Dhakal, R.P. Bi-directional cyclic loading experiment on a 3-D beam–column connection designed for damage avoidance. *J. Struct. Eng.* **2008**, *134*, 1733–1742. [[CrossRef](#)]
23. Pampanin, S.; Amaris, A. Critical aspects in modelling the seismic behavior of precast/ prestressed concrete building connections and systems. In Proceedings of the First FIB Congress, Osaka, Japan, 13–19 October 2002.
24. Youssef, M.A.; Alam, M.S.; Nehdi, M. Experimental investigation on the seismic behavior of beam–column joints reinforced with superelastic shape memory alloys. *J. Earthq. Eng.* **2008**, *12*, 1205–1222. [[CrossRef](#)]
25. Choi, E.; Jeon, J.S.; Lee, J.H. Self-centering capacity of RC columns with smart plastic hinges of martensitic NiTi SMA bars. *Smart Mater. Struct.* **2023**, *32*, 115015. [[CrossRef](#)]
26. Lu, X.L.; Cui, Y.; Liu, J. Shaking table test and numerical simulation of a 1/2-scale self-centering reinforced concrete frame. *Earthq. Eng. Struct. Dyn.* **2015**, *44*, 1899–1917. [[CrossRef](#)]
27. Sun, D.; Yang, Y.; Ma, Y.; Xue, Y.; Yu, Y.; Feng, S. Seismic behavior of self-centering column base with replaceable stiffener angle steels. *Thin-Walled Struct.* **2022**, *181*, 110113. [[CrossRef](#)]
28. Veismoradi, S.; Yousef-beik, S.M.M.; Zarnani, P.; Quenneville, P. Development and parametric study of a new self-centering rotational friction damper. *Eng. Struct.* **2021**, *235*, 112097. [[CrossRef](#)]
29. Song, L.L.; Guo, T.; Gu, Y.; Cao, Z.L. Experimental study of a self-centering prestressed concrete frame subassembly. *Eng. Struct.* **2015**, *88*, 176–188. [[CrossRef](#)]
30. Huang, L.; Zhou, Z.; Huang, X. Variable friction damped self-centering precast concrete beam–column connections with hidden corbels: Experimental investigation and theoretical analysis. *Eng. Struct.* **2020**, *206*, 110150. [[CrossRef](#)]
31. Huang, L.; Clayton, P.M.; Zhou, Z. Seismic design and performance of self-centering precast concrete frames with variable friction dampers. *Eng. Struct.* **2021**, *245*, 112863. [[CrossRef](#)]
32. Rodgers, G.W.; Solberg, K.M.; Chase, J.G.; Mander, J.B.; Bradley, B.A.; Dhakal, R.P. Performance of a damage-protected beam–column subassembly utilizing external HF2V energy dissipation devices. *Earth. Eng. Struct. Dyn.* **2008**, *37*, 1549–1564. [[CrossRef](#)]
33. Rodgers, G.W.; Mander, J.B.; Chase, J.G. Modeling cyclic loading behavior of jointed precast concrete connections including effects of friction, tendon yielding and dampers. *Earthq. Eng. Struct. Dyn.* **2012**, *41*, 2215–2233. [[CrossRef](#)]
34. Kam, W.Y.; Pampanin, S.; Palermo, A.; Carr, A.J. Self-centering structural systems with combination of hysteretic and viscous energy dissipations. *Earthq. Eng. Struct. Dyn.* **2010**, *39*, 1083–1108. [[CrossRef](#)]
35. Huang, L.; Zhou, Z.; Clayton, P.M. Experimental and numerical study of unbonded post-tensioned precast concrete connections with controllable post-decompression stiffness. *Struct. Des. Tall Spec. Build.* **2021**, *30*, e1847. [[CrossRef](#)]
36. Huang, L.; Han, J.; Wen, H.; Li, C.; He, H.; Luo, Y.; Qian, Z. The Seismic Performance and Global Collapse Resistance Capacity of Infilled Reinforced Concrete Frames Considering the Axial–Shear–Bending Interaction of Columns. *Buildings* **2022**, *12*, 2030. [[CrossRef](#)]
37. Zheng, K.; Ni, S.; Zhang, Y.; Gu, J.; Gao, M.; Wei, Y. Post-cracking Shear Stiffness Model of Reinforced Concrete Beams. *Buildings* **2023**, *13*, 2814. [[CrossRef](#)]
38. Zheng, K.; Zhou, S.; Zhang, Y.; Wei, Y.; Wang, J.; Wang, Y.; Qin, X. Simplified Evaluation of Shear Stiffness Degradation of Diagonally Cracked Reinforced Concrete Beams. *Materials* **2023**, *16*, 4752. [[CrossRef](#)]
39. Huang, Z.; Zheng, K.; Wei, Y.; Liu, L.; Tang, X.; Qin, X. Compressive performance of SWSSC-filled CFRP–stainless steel composite tube columns. *Constr. Build. Mater.* **2023**, *385*, 131471. [[CrossRef](#)]
40. Shan, Z.W.; Looi, D.T.; Su, R.K. Confinement model for RC columns strengthened with direct-fastened steel plate. *Steel Compos. Struct.* **2021**, *39*, 367–381.
41. Shan, Z.W.; Su, R.K.L. Flexural capacity model for RC beams strengthened with bolted side-plates incorporating both partial longitudinal and transverse interactions. *Eng. Struct.* **2018**, *168*, 44–57. [[CrossRef](#)]
42. Shan, Z.W.; Looi, D.T.W.; Su, R.K.L. A novel seismic strengthening of RC columns by direct fastening steel plates. *Eng. Struct.* **2020**, *218*, 110838. [[CrossRef](#)]
43. Kam, W.Y.; Pampanin, S.; Carr, A.J. *Design Procedure and Behaviour of Advanced Flag-Shape (AFS) MDOF Systems*; New Zealand Society for Earthquake Engineering (NZSEE): Wellington, New Zealand, 2008; pp. 1–18.
44. GB50011-2010; Code for Seismic Design of Buildings. National Standards of the People’s Republic of China: Beijing, China, 2010. (In Chinese)

45. Du, H.; Liu, J.; Yuan, S. Mechanical behavior of glulam-concrete composite beam with notched connections under ISO 834 standard fire. *J. Build. Eng.* **2023**, *78*, 107670. [[CrossRef](#)]
46. Du, H.; Yuan, S.; Yu, T.; Hu, X. Experimental and analytical investigation on flexural behavior of high-strength steel-concrete composite beams. *Buildings* **2023**, *13*, 902. [[CrossRef](#)]

Disclaimer/Publisher's Note: The statements, opinions and data contained in all publications are solely those of the individual author(s) and contributor(s) and not of MDPI and/or the editor(s). MDPI and/or the editor(s) disclaim responsibility for any injury to people or property resulting from any ideas, methods, instructions or products referred to in the content.